

Irreversibility and Chaos in Active Particle Suspensions

Sergio Chibbaro

*Sorbonne Universit, Centre National de la Recherche Scientifique,
UMR 7190, Institut Jean Le Rond d'Alembert, F-75005 Paris, France*

Astrid Decoene

*Universit Paris Sud, Laboratoire de mathématiques d'Orsay
(CNRS-UMR 8628), Bâtiment 425, 91405 Orsay cedex, France**

Sebastien Martin

*Universit Paris Descartes, Laboratoire MAP5 (CNRS UMR 8145),
45 rue des Saints-Pères, 75270 Paris cedex 06, France*

Fabien Vergnet

*Universit Paris Sud, Laboratoire de mathématiques d'Orsay
(CNRS-UMR 8628), Bâtiment 425, 91405 Orsay cedex, France*

Active matter has been the object of huge amount of research in recent years for its important fundamental and applicative properties. In this paper we investigate active suspensions of microswimmers through direct numerical simulation, so that no approximation is made at the continuous level other than the numerical one. We consider both pusher and puller organisms, with a spherical or ellipsoidal shape. We analyse the velocity and the characteristic scales for an homogeneous two-dimensional suspension and the effective viscosity under shear. We bring evidences that the complex features displayed are related to a spontaneous breaking of the time-reversal symmetry. We show that chaos is not a key ingredient, whereas a large enough number of interacting particles and a non-spherical shape are needed to break the symmetry and are therefore at the basis of the phenomenology. Our numerical study also shows that pullers display some collective motion, though with different characteristics from pushers.

Introduction Active matter is one of the major subjects of physical research because of its relevance in medicine, ecology and its possible applications [2, 30, 31, 36, 49, 52]. In nature, many living organisms swim through fluids at low Reynolds (Re) number [47]. A particularly interesting instance of such low-Reynolds number world is given by a suspension of self-propelled particles, also called swimmers [32, 44], which are essential in life-cycle [42] as well as in bio-engineering [16]. These small objects can exhibit complex dynamics as a result of the long-ranged hydrodynamic interactions which stem from the swimming activity, unfolding large-scale motion characterised by a various phenomenology of patterns, as highlighted in numerous experiments [13, 41, 45, 48, 51, 56]. More specifically, bacteria may produce mesoscopic patterns of collective motion sometimes called bio-turbulence [14, 35, 54, 57]. In a flow, these bacteria may organize spatially and under shear they yield the possibility to increase or decrease the macroscopic viscosity to values above or below the suspending fluid viscosity, depending on their geometry and type of activity. To understand the motion of such self-propelled particles, it has been analysed in numerical mod-

els, which are able to capture salient features of experiments, including hydrodynamic diffusion, large-scale collective motions and strong density fluctuations [15, 24, 52, 53, 60, 64]. Yet, different level of approximation either on the interactions or on the size of the objects are introduced to limit the computational cost, and the precise mechanisms underlying the phenomenology remain to be fully understood [7, 19, 55]. In this work, we develop a direct numerical approach that does not make use of any approximation other than considering a continuous medium, and we focus on a striking feature of low-Re number flows, its reversibility in time [47, 61]. As emphasised in statistical mechanics since Boltzmann [5, 9, 20], the relation between microscopic dynamics and macroscopic properties hides subtle issues, notably concerning the role of chaos and number of degrees of freedom [11, 33]. It has been shown that non-Brownian passive suspensions break the time-reversal symmetry at the level of single particles, even though they are governed by reversible creeping equations [46]. Identifying the mechanisms underlying breaking of time-reversal symmetry in biological swimmers and relate that to the macroscopic turbulent properties is the goal of this letter. In par-

ticular, we bring evidence of a spontaneous breaking of the time-reversal symmetry, for which the key ingredients are: (i) a number of particles large enough to trigger important non-linear interactions among particles; (ii) an elongated shape of the particles. It is important to underline here that if only the first condition is fulfilled, a complex “bio-turbulent” behaviour with large-scale collective motion is still encountered but the system remains reversible in time, showing no differences between spherical pushers and pullers and no particular rheological signature.

Theoretical Model We model each micro-organism as a rigid ellipsoidal or spherical particle moving in the fluid. The flagella or cilia are not materialized; we only take into account the resultant force they exert on the particles and on the fluid. We deal with two kinds of flagellated swimmers, “Pushers”, such as *Bacillus subtilis* or *Escherichia coli*, whose flagellar apparatus is localized at the back of the cell body, and “pullers” such as *Chlamydomonas reinhardtii*, which typically propel themselves through flagella attached at the front of their cell body that execute a breaststroke-like motion [52]. In fact, the complex movement of the locomotion structures (flagellar bundle or cilia) results in an effective force acting on the fluid in a zone with non-zero volume, downstream (in the case of pushers), or upstream (in the case of pullers) of the organism. The modelled organisms are sketched in Fig. 1, where the model is presented.

A suspension of concentration ϕ is modeled by N swimmers for the sake of simplicity in a two-dimensional domain $\Omega = L^2$. At the initial time the particles are distributed randomly over the fluid (without overlapping). The position of the center of the i th particle is denoted by \mathbf{x}_i , and by \mathbf{v}_i and ω_i its translational and angular velocities. We describe the fluid flow by the Stokes equations :

$$\begin{cases} -\mu\Delta\mathbf{u} + \nabla p = \mathbf{f}_f \\ \nabla \cdot \mathbf{u} = 0 \end{cases} \quad (1)$$

where $\mathbf{u} = (u_1, u_2)$ and p are the velocity and pressure field in the fluid. This system is completed by specific boundary conditions: no-slip boundary conditions on the boundary ∂B_i of each rigid particle, and periodic conditions on $\partial\Omega$, if not differently specified. The forces considered on the fluid are the forces exerted by the locomotion structure. Newton’s second law of motion governs the dynamics of the rigid bodies: force and torque balances are applied on each particle B_i (see supplemental material for details). The motion of each bacterium B_i is then set by its instantaneous veloc-

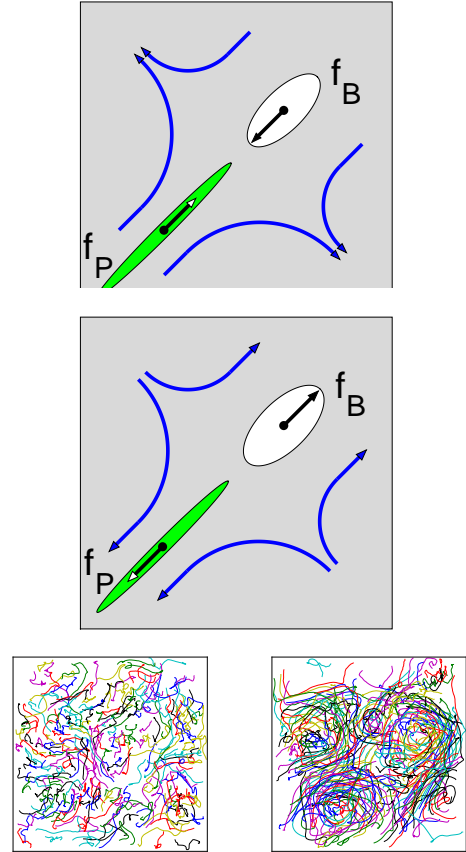


FIG. 1. Each bacterium is modeled by a rigid body B , with an associated propulsion force \mathbf{f}_B , and the action of the flagellar bundle over the fluid is located inside a fluid region P which can be deduced from the position of the rigid body. The propulsion is such that the total force exerted by the swimmer on the fluid is equal to the total force of the fluid on the particle. The propulsion force \mathbf{f}_B is directed outward from the center of B , parallel to the semi-major axes of B and P , and has some orientation angle θ . The two types of swimmers are modeled in this way: *pushers* (right panels) push themselves forward by using flagella set back on the body; *pullers* (left panels) pull themselves forward as they swim flagella first and generate the opposite flow field. More details on the model can be found in supplemental material [10]. Bottom: Swimmer displacements/trajectories in the homogeneous bi-periodic flow, after the transient period and with a volume fraction of $\phi = 0.3$.

ity, $\mathbf{u}(\mathbf{x}, t) = \mathbf{v}_i(t) + \omega_i(t) \times (\mathbf{x} - \mathbf{x}_i(t))$ defined in B_i , and the dynamics by the differential equations: $\dot{\mathbf{x}}_i(t) = \mathbf{v}_i(t)$, $\dot{\theta}_i(t) = \omega_i(t)$. We use random values for the initial data $\mathbf{x}_i(t=0)$ and $\theta_i(t=0)$. The coupled fluid-particle problem is solved using the finite element method applied to solve the Stokes problem in the whole domain Ω , and a penalty method to

enforce the rigid motion constraint inside the rigid domain B . Possible numerical overlap between rigid particles due to the numerical errors must be prevented in order to guarantee robustness of the simulations. We have extended the numerical method previously proposed for granular gases [37], where inelastic collisions between rigid particles are computed. More details on the numerical method are given in the supplemental material [10].

Numerical results In Fig. 1, we show the trajectories obtained by the simulation of pushers and pullers with elongated ellipsoidal shape. It is apparent that the dynamics is highly nontrivial in both cases, being characterised by very irregular displacements which highlight the nonlinear interaction among swimmers which produce a chaotic motion. Yet, the two configurations show differences in the collective motion: pushers are able to build large rolls, as found also experimentally [13], while pullers appear to be coherent on smaller times, but are nonetheless found to be able to form collective rolls, though weaker than pushers, see [10] for a movie. Swimmers tend therefore to form local inhomogeneities and to some extent synchronize their time trajectories, as found also in stochastic models [50, 62].

To analyse quantitatively this issue, we have investigated the root mean square velocity of the organisms as displayed in Fig. 2. It shows that the collective flow speed can be highly increased by hydrodynamic interactions in moderate to dense suspensions for both swimmers, and up to one order of magnitude for pushers consistent with experimental observations [58]. Pushers are found to create stronger collective velocity than pullers, when the solid fraction is higher than few percents and elongated shape is taken into account. In dilute suspensions, swimmers are basically isolated and the dynamics is the same for all species. The difference reaches a maximum at a concentration of around 20%, and then decreases at higher concentration due to congestion in dense suspensions, resulting in the close-pack structural configuration of the rigid micro-swimmers [13]. Remarkably, when the numerical experiment is performed with spheres the difference in the mean velocity is within the numerical errors. Moreover, the mean velocity of the spheres is situated between ellipsoidal pushers and pullers. Looking at the velocity correlation, we have found that ellipsoidal pushers exhibit the most important local alignment, which explains the increase in velocity and larger coherent structures, whose typical length turns out to be about $0.3L$. Spherical pullers and pushers show the

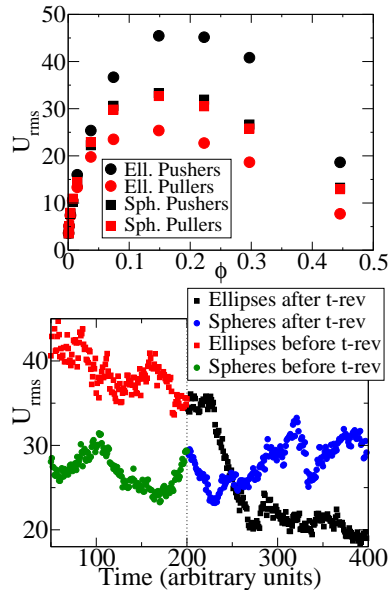


FIG. 2. Top: Rms velocity defined as $U_{rms} \equiv \sqrt{\langle U^2 \rangle}$ of the suspension, for pushers and pullers at different concentration, from dilute to dense suspensions. Both populations of swimmers have been studied with ellipsoidal and spherical shape. The velocity of the single particle is such that $U_{rms} \approx 1$. Bottom: We plot the root-mean-square velocity computed over all particles at each time-step for a suspension of pushers, both for ellipsoidal and spherical particles, for a concentration of $\phi = 0.3$. At the time $t_0 = 200$ the dynamics is inverted, which means $t \rightarrow -t$ and $\mathbf{V} \rightarrow -\mathbf{V}$.

same properties, being reversible in time. In all cases some alignment is found, showing that pullers are also responsible for some structures even though of less importance [10]. This differentiation suggests a time-symmetry breaking due to collective behaviour since applying the time-reversal operator to pullers one obtains formally the pusher dynamics and vice-versa. To highlight the issue, we have made the following experiment: we start a simulation with a pusher suspension, and at time t_0 we reverse the dynamics with a round-off error of 10^{-16} . In principle, given that the system is reversible, it should retrace its steps. It turns out that for ellipsoidal shape after a small amount of time in which the dynamics is reversed within numerical errors, the system breaks the time-symmetry, as shown in the Fig.2b. Instead, for spherical active particles, the forward and backward time-trajectory is practically indistinguishable, at least from a statistical point of view.

The irregular motion displayed in Fig. 1 suggests also that swimmers are sensitive to small changes in the initial conditions, that is they are chaotic in

the sense of a positive Maximum Lyapunov exponent (LE) [8, 43]. Since in some cases the macroscopic irreversibility has been related to chaos [39, 40, 46], we quantify this sensitivity computing the LE λ for the two species of bacteria for different concentrations, both for ellipsoidal and spherical shape. The LE is computed from the Euclidean distance between two simulations labelled 1,0 as $\Delta(t) = \frac{1}{N} \sqrt{\sum_{i=1}^N (x_i^1 - x_i^0)^2 + (y_i^1 - y_i^0)^2}$. The initial difference between the two simulations is set $\delta \mathbf{x}(t=0) = 10^{-8}$ on only one particle, and for chaotic systems, Δ grows exponentially as $|\delta \mathbf{x}| \exp(\lambda t)$. All the cases are chaotic, except in the dilute regime where particles do not interact, and it is clear that shape does not play any role in chaos, as found also for passive particles [28, 29, 39, 46]. Indeed, for a given concentration we have not measured any difference neither changing shape neither between puller and pusher. A dependence on ϕ is yet found: $\lambda \approx 0.1 \pm 0.01$ for $\phi \lesssim 0.2$ and $\lambda \approx 0.3 \pm 0.02$ for $\phi \gtrsim 0.2$. Two mechanisms in principle can lead to such a chaotic behaviour, the N-body hydrodynamical interactions and the pair-contact ones. We have nevertheless verified that our results are insensitive to contacts, as already shown by the correct reversibility of spherical objects. We also assure a such small time-step that particles do not reach each other except in very rare cases. Furthermore, the amplification is almost the same even without taking into account the contacts, as already shown in sheared suspensions [40]. Hence, long-range hydrodynamic interactions lead to a chaotic regime, but chaos does not play any role in the macroscopic irreversibility.

We analyse now some of the rheology characteristics of swimmer suspensions. We focus on the study of the shear-viscosity in a fluid confined between two parallel rigid plates with a steady relative shear motion. In this case one can measure the shear stress, which is defined as the average force applied by the fluid on the plates per surface unit in response to this shear $F = \int_{\Gamma} (\boldsymbol{\sigma} \cdot \mathbf{n}) \cdot \boldsymbol{\tau} / 2L$ where Γ denotes the surface of the two plates, L denotes the length of each plate, \mathbf{n} is the normal vector Γ pointing outward and $\boldsymbol{\tau}$ is the tangential vector on Γ opposed to the shear flow. Consequently, for a suspension, an apparent viscosity is defined as $\mu_{\text{app}}(t) = F/\dot{\gamma}$, where $\dot{\gamma}$ denotes the shear rate. Since this value changes in time due to the evolution of the particles configuration, one usually considers the effective viscosity: $\mu_{\text{eff}} = \lim_{T \rightarrow +\infty} \frac{1}{T} \int_0^T \mu_{\text{app}}(t) dt$. We have computed the effective viscosity in active suspensions of pusher- and puller-like swimmers using

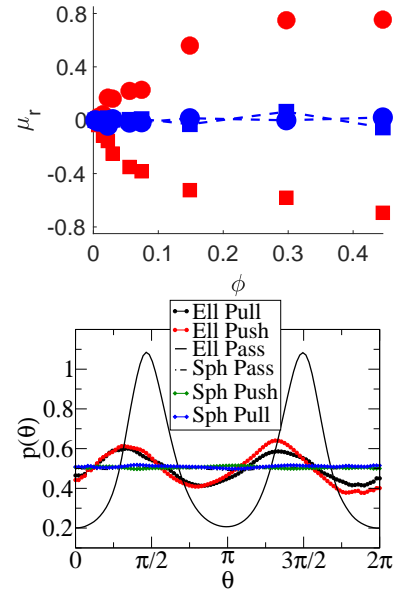


FIG. 3. (a) Evolution with the concentration in a suspension of ellipsoidal pushers and pullers of the relative effective viscosity $\mu_r = (\mu - \mu_{\text{passive}})/\mu_{\text{passive}}$, where μ_{passive} is the effective viscosity of the suspension for non-active particles. Pushers are indicated by the symbol \square , and Pullers by \bullet . Red symbols indicate elongated particles, while blue-dashed ones are for spherical particles. (b) Probability density function of orientations in the simulations of pusher, puller and passive suspensions. The concentration is $\phi = 0.15$ and the ellipsoidal particles are of elongation ratio 2.

2D simulations in which shear is imposed through non-homogenous Dirichlet conditions at walls and periodic boundary conditions are imposed on the left and right boundaries. It is well known that the viscosity of a passive suspension of particles is different from that of the solvent [1, 17, 18], and that shape of the particles has an effect [6]. We analyse here the impact of the active (swimming) motion looking at the effective relative viscosity, that is eliminating the rheology signature related to the passive suspension, see Fig. 3. Beyond the dilute regime, elongated pusher-like swimmers tend to decrease the effective viscosity, while pullers increase it [22]. Yet spherical ones have no relative rheological signature, spherical active particles behaving like the passive ones [23, 26, 52]. Furthermore, puller and pushers act in a symmetrical way with respect to the corresponding spherical suspensions, as highlighted by Fig. 3. As shown in Fig. 3b, physically, the broken symmetry by elongation translates into a preferential alignment in the flow at positions which maximise (minimise) the effective viscosity for Pullers

(Pushers). Passive ellipses have preferential alignment but symmetrical with respect to the neutral position. Spheres are not able to break the symmetry and do not show any preferential alignment. See the supplemental material for more details. Our study shows again that, if no other mechanism is added, elongation is needed to produce an additional rheological signature, which points out again the link to spontaneous symmetry breaking by shape.

Conclusions We have reported on numerical experiments of swimmer dynamics obtained without other approximations than the hydrodynamics, the fluid-structure interaction being explicitly accounted for. The simulations are able to reproduce all the relevant dynamical features. We have shown unambiguously that all the features characteristic of the collective bio-turbulent regime may be related to the following ingredients: the number of active particles and the elongation. The former is necessary to trigger interactions between velocities which in turn provoke a chaotic motion. In particular, alignment of particles are obtained, even without explicit interaction between directions. Elongation allows to spontaneously break the symmetry under time-reversal which explains the observed impact both on motion and rheology. Interestingly, Pullers are found to produce "bio-turbulence", even though of less entity than pushers. Simplified models and artificial devices could be based upon these conclusions.

* astrid.decoene@math.orsay.fr

- [1] G. Batchelor. The effect of brownian motion on the bulk stress in a suspension of spherical particles. *Journal of fluid mechanics*, 83(1):97–117, 1977.
- [2] C. Bechinger, R. Di Leonardo, H. Löwen, C. Reichhardt, G. Volpe, and G. Volpe. Active particles in complex and crowded environments. *Reviews of Modern Physics*, 88(4):045006, 2016.
- [3] M. Belzons, R. Blanc, J. L. Bouillot, and C. Camoin. Viscosité d’une suspension diluée et bidimensionnelle de sphères. *C. R. Acad. Sci, Paris II*, 292:939–44, 1981.
- [4] H. C. Berg. *Random walks in biology*. Princeton University Press, 1983.
- [5] L. Boltzmann. *Lectures on gas theory*. Courier Corporation, 2012.
- [6] H. Brenner. Rheology of a dilute suspension of axisymmetric brownian particles. *International journal of multiphase flow*, 1(2):195–341, 1974.
- [7] L. Caprini, U. M. B. Marconi, and A. Puglisi. Spontaneous velocity alignment in motility-induced phase separation. *Phys. Rev. Lett.*, 124(7):078001, 2020.
- [8] M. Cencini, F. Cecconi, and A. Vulpiani. *Chaos: from simple models to complex systems*, volume 17. World Scientific, 2010.
- [9] C. Cercignani. *The Boltzmann equation*. Springer, 1988.
- [10] S. Chibbaro, A. Decone, S. Martin, and F. Vergnet. *Supplemental Material*.
- [11] S. Chibbaro, L. Rondoni, and A. Vulpiani. *Reductionism, emergence and levels of reality*. Springer, 2014.
- [12] P. G. Ciarlet. *Introduction à l’analyse numérique matricielle et à l’optimisation*. Masson. Paris, 1990.
- [13] L. H. Cisneros, J. O. Kessler, S. Ganguly, and R. E. Goldstein. Dynamics of swimming bacteria: Transition to directional order at high concentration. *Physical Review E*, 83(6):061907, 2011.
- [14] C. Dombrowski, L. Cisneros, S. Chatkaew, R. E. Goldstein, and J. O. Kessler. Self-concentration and large-scale coherence in bacterial dynamics. *Physical Review Letters*, 93(9):098103, 2004.
- [15] K. Drescher, J. Dunkel, L. H. Cisneros, S. Ganguly, and R. E. Goldstein. Fluid dynamics and noise in bacterial cell–cell and cell–surface scattering. *Proceedings of the National Academy of Sciences*, 108(27):10940–10945, 2011.
- [16] R. Dreyfus, J. Baudry, M. L. Roper, M. Fermigier, H. A. Stone, and J. Bibette. Microscopic artificial swimmers. *Nature*, 437(7060):862–865, 2005.
- [17] A. Einstein. Einenenu bestimmungder molekuldimensionen. *Ann. Physik*, pages 19–289, 1906.
- [18] A. Einstein. Berichtigung zu meiner arbeit: Eine neue bestimmung der moleküldimensionen. *Annalen der Physik*, 339(3):591–592, 1911.
- [19] Y. Fily and M. C. Marchetti. Athermal phase separation of self-propelled particles with no alignment. *Physical review letters*, 108(23):235702, 2012.
- [20] G. Gallavotti. *Nonequilibrium and irreversibility*. Springer, 2014.
- [21] D. Gérard-Varet and M. Hillairet. Regularity issues in the problem of fluid structure interaction. *Arch. Ration. Mech. Anal.*, 195(2):375–407, 2010.
- [22] V. Gyrya, K. Lipnikov, I. S. Aranson, and L. Berlyand. Effective shear viscosity and dynamics of suspensions of micro-swimmers from small to moderate concentrations. *J. Math. Biol.*, 62(5):707–740, 2011.
- [23] B. M. Haines, I. S. Aranson, L. Berlyand, and D. A. Karpeev. Effective viscosity of dilute bacterial suspensions: a two-dimensional model. *Phys. Biol.*, 5(4):046003, 2008.
- [24] J. P. Hernandez-Ortiz, C. G. Stoltz, and M. D. Graham. Transport and collective dynamics in suspensions of confined swimming particles. *Physical review letters*, 95(20):204501, 2005.
- [25] M. Hillairet. Lack of collision between solid bodies in a 2D incompressible viscous flow. *Comm. Partial Differential Equations*, 32(7-9):1345–1371, 2007.
- [26] T. Ishikawa and T. J. Pedley. The rheology of a semi-dilute suspension of swimming model microorganisms. *J. Fluid Mech.*, 588:399–435, 10 2007.

- [27] J. Janela, A. Lefebvre, and B. Maury. A penalty method for the simulation of fluid-rigid body interaction. *ESAIM: Proc.*, 1:115–123, 2005.
- [28] I. M. Jánosi, T. Tél, D. E. Wolf, and J. A. Galas. Chaotic particle dynamics in viscous flows: The three-particle stokeslet problem. *Physical Review E*, 56(3):2858, 1997.
- [29] G. Károlyi, Á. Péntek, I. Scheuring, T. Tél, and Z. Toroczkai. Chaotic flow: the physics of species coexistence. *Proceedings of the National Academy of Sciences*, 97(25):13661–13665, 2000.
- [30] D. L. Koch and G. Subramanian. Collective hydrodynamics of swimming microorganisms: living fluids. *Annual Review of Fluid Mechanics*, 43:637–659, 2011.
- [31] E. Lauga. Bacterial hydrodynamics. *Annual Review of Fluid Mechanics*, 48:105–130, 2016.
- [32] E. Lauga and T. R. Powers. The hydrodynamics of swimming microorganisms. *Reports on Progress in Physics*, 72(9):096601, 2009.
- [33] J. L. Lebowitz. Boltzmann’s entropy and time’s arrow. *Physics today*, 46(9):32–38, 1993.
- [34] A. Lefebvre. Fluid-particle simulations with freefem++. In *Esaim: Proceedings*, volume 18, pages 120–132. EDP Sciences, 2007.
- [35] H. M. López, J. Gachelin, C. Douarache, H. Auradou, and E. Clément. Turning bacteria suspensions into superfluids. *Physical review letters*, 115(2):028301, 2015.
- [36] M. C. Marchetti, J.-F. Joanny, S. Ramaswamy, T. B. Liverpool, J. Prost, M. Rao, and R. A. Simha. Hydrodynamics of soft active matter. *Reviews of Modern Physics*, 85(3):1143, 2013.
- [37] B. Maury. A time-stepping scheme for inelastic collisions. Numerical handling of the nonoverlapping constraint. *Numer. Math.*, 102(4):649–679, 2006.
- [38] B. Maury. Numerical analysis of a finite element / volume penalty method. *SIAM J. Numer. Anal.*, 47:1126–1148, 2009.
- [39] B. Metzger and J. E. Butler. Irreversibility and chaos: Role of long-range hydrodynamic interactions in sheared suspensions. *Physical Review E*, 82(5):051406, 2010.
- [40] B. Metzger, P. Pham, and J. E. Butler. Irreversibility and chaos: Role of lubrication interactions in sheared suspensions. *Physical Review E*, 87(5):052304, 2013.
- [41] G. Mino, T. E. Mallouk, T. Darnige, M. Hoyos, J. Dauchet, J. Dunstan, R. Soto, Y. Wang, A. Rouselet, and E. Clement. Enhanced diffusion due to active swimmers at a solid surface. *Physical review letters*, 106(4):048102, 2011.
- [42] W. H. Munk. Abyssal recipes. In *Deep Sea Research and Oceanographic Abstracts*, volume 13, pages 707–730. Elsevier, 1966.
- [43] E. Ott. *Chaos in dynamical systems*. Cambridge university press, 2002.
- [44] T. Pedley and J. Kessler. Hydrodynamic phenomena in suspensions of swimming microorganisms. *Annual Review of Fluid Mechanics*, 24(1):313–358, 1992.
- [45] A. P. Petroff, X.-L. Wu, and A. Libchaber. Fast-moving bacteria self-organize into active two-dimensional crystals of rotating cells. *Physical review letters*, 114(15):158102, 2015.
- [46] D. Pine, J. P. Gollub, J. Brady, and A. Leshansky. Chaos and threshold for irreversibility in sheared suspensions. *Nature*, 438(7070):997–1000, 2005.
- [47] E. M. Purcell. Life at low reynolds number. *American journal of physics*, 45(1):3–11, 1977.
- [48] S. Rafai, L. Jibuti, and P. Peyla. Effective viscosity of microswimmer suspensions. *Physical Review Letters*, 104(9):098102, 2010.
- [49] S. Ramaswamy. The mechanics and statistics of active matter. *Annu. Rev. Condens. Matter Phys.*, 1(1):323–345, 2010.
- [50] P. Romanczuk, M. Bär, W. Ebeling, B. Lindner, and L. Schimansky-Geier. Active brownian particles. *The European Physical Journal Special Topics*, 202(1):1–162, 2012.
- [51] R. Rusconi, J. S. Guasto, and R. Stocker. Bacterial transport suppressed by fluid shear. *Nature physics*, 10(3):212–217, 2014.
- [52] D. Saintillan. Rheology of active fluids. *Annual Review of Fluid Mechanics*, 50:563–592, 2018.
- [53] D. Saintillan and M. J. Shelley. Instabilities and pattern formation in active particle suspensions: kinetic theory and continuum simulations. *Physical Review Letters*, 100(17):178103, 2008.
- [54] D. Saintillan and M. J. Shelley. Emergence of coherent structures and large-scale flows in motile suspensions. *Journal of the Royal Society Interface*, 9(68):571–585, 2012.
- [55] E. Sese-Sansa, I. Pagonabarraga, and D. Levis. Velocity alignment promotes motility-induced phase separation. *EPL (Europhysics Letters)*, 124(3):30004, 2018.
- [56] A. Sokolov and I. S. Aranson. Reduction of viscosity in suspension of swimming bacteria. *Physical Review Letters*, 103(14):148101, 2009.
- [57] A. Sokolov, I. S. Aranson, J. O. Kessler, and R. E. Goldstein. Concentration dependence of the collective dynamics of swimming bacteria. *Physical Review Letters*, 98(15):158102, 2007.
- [58] A. Sokolov, I. S. Aranson, J. O. Kessler, and R. E. Goldstein. Concentration dependence of the collective dynamics of swimming bacteria. *Phys. Rev. Lett.*, 98:158102, 2007.
- [59] C. A. Solari, J. O. Kessler, and R. E. Goldstein. Motility, mixing, and multicellularity. *Genet. Program Evol. M.*, 8(2):115–129, 2007.
- [60] J. Stenhammar, C. Nardini, R. W. Nash, D. Marenduzzo, and A. Morozov. Role of correlations in the collective behavior of microswimmer suspensions. *Physical review letters*, 119(2):028005, 2017.
- [61] G. Taylor and J. Friedman. Low reynolds number flows (national committee on fluid mechanics films), 1966.
- [62] B. ten Hagen, S. van Teeffelen, and H. Löwen. Brownian motion of a self-propelled particle. *Journal of Physics: Condensed Matter*, 23(19):194119, 2011.

- [63] S. Vincent, J. Caltagirone, P. Lubin, and T. N. Randeria. An adaptative augmented Lagrangian method for three-dimensional multimaterial flows. *Computers and Fluids*, 33:1273–1289, 2004.
- [64] H. H. Wensink, J. Dunkel, S. Heidenreich, K. Drescher, R. E. Goldstein, H. Löwen, and J. M. Yeomans. Meso-scale turbulence in living fluids. *Proceedings of the National Academy of Sciences*, 109(36):14308–14313, 2012.

SUPPLEMENTAL MATERIAL

MODEL

In this section, we briefly describe the continuous model used. Each swimmer's body is represented by a rigid ellipsoid B , to which we associate a dipole of forces, homogeneously distributed inside the rigid body and inside an elongated ellipsoidal region P in the fluid, placed at a constant distance from the bacterial body and representing the location of the flagella appendage, see Fig. S4. The propulsion force exerted on the body of each swimmer i is denoted by \mathbf{F}_{B_i} , has constant magnitude f_P and is directed outward from the center of B_i , parallel to the majorsemiaxes of B_i and P_i . It has some orientation angle θ_i , as shown in Fig. S4(A), and satisfies :

$$\mathbf{F}_{B_i} = f_P \boldsymbol{\tau}_i = \int_{B_i} \mathbf{f}_{B_i} d\mathbf{x}, \quad \text{with} \quad \mathbf{f}_{B_i} = \frac{f_P}{|B_i|} \boldsymbol{\tau}_i,$$

where $\boldsymbol{\tau}_i$ is given by the orientation angle θ_i . Since each swimmer is force and torque-free, the total force exerted by the swimmer on the fluid is equal to $-\mathbf{F}_{B_i}$, and we can write:

$$\mathbf{F}_{P_i} = -f_P \boldsymbol{\tau}_i = \int_{P_i} \mathbf{f}_{P_i} d\mathbf{x}, \quad \text{with} \quad \mathbf{f}_{P_i} = -\frac{f_P}{|P_i|} \boldsymbol{\tau}_i.$$

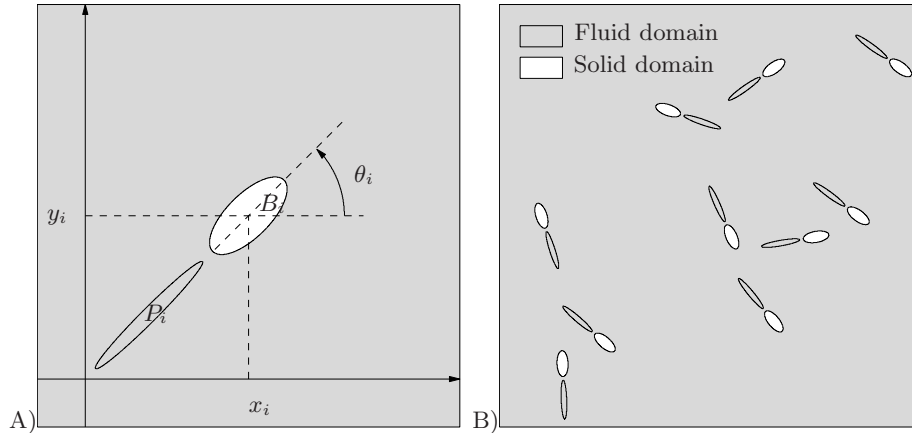


FIG. S4. A) Domain Ω is made of a solid domain B (collection of rigid bodies of the bacteria) and a fluid domain $\Omega \setminus B$. Denoting by $(B_i)_{i=1, \dots, N}$ the rigid particles representing the body of the swimmers, strongly included in Ω , and by $B = \cup_i B_i$ the whole rigid domain, the suspension has a volume concentration of $\phi = |B|/|\Omega|$, where $|\omega|$ denotes the measure of a domain ω . B) Each bacterium is modeled by a rigid body B_i . Its position is characterized by the coordinates $\mathbf{x}_i = (x_i, y_i)$ of its center of mass and its orientation θ_i . The action of the flagellar bundle over the fluid is located at a fluid region P_i which can be deduced from the position of the rigid body.

The Reynolds number is typically less than 10^{-2} [4, 59], therefore inertial effects can be neglected and the fluid flow is described by the Stokes equations :

$$\begin{cases} -\nabla \cdot \underline{\underline{\sigma}}(\mathbf{u}, p) = \mathbf{f}_f & \text{in } \Omega \setminus \bar{B}, \\ \nabla \cdot \mathbf{u} = 0 & \text{in } \Omega \setminus \bar{B}, \end{cases} \quad (\text{S2})$$

where \mathbf{u} and p are the velocity and pressure field in the fluid, and where the stress tensor $\underline{\underline{\sigma}}$ writes

$$\underline{\underline{\sigma}} = 2\mu \mathbb{D}(\mathbf{u}) - p \mathbb{I}, \quad \text{where} \quad \mathbb{D}(\mathbf{u}) = \frac{\nabla \mathbf{u} + (\nabla \mathbf{u})^T}{2}$$

since we consider a Newtonian fluid. This system is completed by specific boundary conditions: no-slip boundary conditions on the boundary ∂B_i of each rigid particle and some Dirichlet or periodic conditions on

$\partial\Omega$. The forces considered on the fluid are the forces exerted by the flagella:

$$\mathbf{f}_f = \sum_{i=1, \dots, N} \mathbf{f}_{P_i} \chi_{P_i},$$

where χ_{P_i} is the characteristic function associated to the region P_i and χ_{B_i} is the characteristic function associated to the particle B_i . Finally, force and torque balance for each body writes:

$$\left\{ \begin{array}{l} \int_{B_i} \rho \mathbf{g} + \int_{B_i} \mathbf{f}_{B_i} - \int_{\partial B_i} \underline{\underline{\sigma}} \cdot \mathbf{n} = 0 \quad \forall i \in \{1, \dots, N\}, \\ \int_{\partial B_i} (\mathbf{x} - \mathbf{x}_i) \times \underline{\underline{\sigma}} \cdot \mathbf{n} = 0 \quad \forall i \in \{1, \dots, N\}, \end{array} \right. \quad (\text{S3})$$

where ρ denotes the buoyant density of swimmers, which is positive since these are slightly denser than the fluid, and $\mathbf{g} = (0, -g)$ is gravity.

The motion of each bacterium B_i is then set by its instantaneous velocity:

$$\mathbf{u}(\mathbf{x}, t) = \mathbf{v}_i(t) + \omega_i(t) \times (\mathbf{x} - \mathbf{x}_i(t))$$

defined on ∂B_i . More precisely, the individual translational velocity is equal to the average velocity:

$$\mathbf{v}_i(t) = \frac{1}{|\partial B_i(t)|} \int_{\partial B_i} \mathbf{u}(t, \mathbf{x}) \, d\mathbf{x}, \quad (\text{S4})$$

and the individual angular velocity is equal to

$$\omega_i(t) = \frac{1}{|\partial B_i(t)|} \frac{\int_{\partial B_i} \mathbf{u}(t, \mathbf{x}) \times (\mathbf{x} - \mathbf{x}_i(t)) \, d\mathbf{x}}{\int_{\partial B_i} |\mathbf{x} - \mathbf{x}_i(t)|^2 \, d\mathbf{x}}. \quad (\text{S5})$$

The swimmers dynamics are then set by the differential equations:

$$\dot{\mathbf{x}}_i(t) = \mathbf{v}_i(t), \quad \dot{\theta}_i(t) = \omega_i(t). \quad (\text{S6})$$

These introduce a dependency in time into the problem: Stokes equations are steady, but their solution depends on time because the configuration of the swimmers inside the fluid varies in time.

NUMERICAL SCHEME

The coupled fluid-particle problem is solved using a new specific finite element method applied to solve the Stokes problem in the whole domain Ω , and a penalty method to enforce the rigid motion constraint inside the rigid domain B . This method is rigorous in the sense that the numerical solution mathematically converges to the solution of the fluid-structure problem as the penalty parameter tends to 0. The time algorithm reads as follows: in a first step, the fluid-particle problem is solved without taking into account the possible overlapping of the particles (thus defining an *a priori* velocity of the swimmers), then the projection of this *a priori* velocity onto the set of admissible velocities is computed. Finally, the position and orientation of each swimmer is updated. The position and orientation of each swimmer at time t^{n+1} are updated by solving the ODEs (S6) using for instance a second-order Adam-Bashfort method. A brief description of the schemes are given in the following.

A fictitious domain approach

The fictitious domain approach we use allows to avoid remeshing. We use a penalty method: the rigid motion constraint is obtained by relaxing a term in the variational formulation, what amounts to replace rigid zones by highly viscous ones (see [27, 34, 63]). The mathematical problem is solved in the following constrained functional spaces:

$$K_{\nabla} = \{\mathbf{u} \in H_0^1(\Omega), \nabla \cdot \mathbf{u} = 0\}, \quad K_B = \{\mathbf{u} \in H_0^1(\Omega), \mathbb{D}(\mathbf{u}) = 0 \text{ a.e. in } B\}.$$

K_{∇} is the space of divergence free functions defined on Ω and K_B is the space of functions which do not deform B . The solution to the initial problem, defined on $\Omega \setminus \bar{B}$, can be extended on the whole domain Ω by a function in K_B : $\mathbf{u}(\mathbf{x}, \cdot) = \mathbf{v}_i + \omega_i \times (\mathbf{x} - \mathbf{x}_i)$ in B_i for every i , and we still denote this extension by \mathbf{u} . The problem in variational form can then be written as the minimization of the functional

$$J(\mathbf{u}) = \mu \int_{\Omega} |\mathbb{D}(\mathbf{u})|^2 - \int_{\Omega} \mathbf{f} \cdot \mathbf{u}$$

on $K_B \cap K_{\nabla}$, where

$$\mathbf{f} = \sum_{i=1}^N (\mathbf{f}_b^i \chi_b^i + \mathbf{f}_p^i \chi_p^i).$$

The rigid motion constraint is relaxed by introducing the following penalty term in the functional to minimize:

$$\int_B \frac{1}{\varepsilon} \mathbb{D}(\mathbf{u}) : \mathbb{D}(\mathbf{u}),$$

so that $\mathbb{D}(\mathbf{u})$ goes to zero in B when ε goes to zero and \mathbf{u} tends to a rigid motion in B . The variational formulation obtained is: find $\mathbf{u}_{\varepsilon} \in H_0^1(\Omega)$ and $p \in L_0^2(\Omega)$ such that

$$\begin{cases} 2\mu \int_{\Omega} \mathbb{D}(\mathbf{u}_{\varepsilon}) : \mathbb{D}(\tilde{\mathbf{u}}) + \frac{2}{\varepsilon} \int_B \mathbb{D}(\mathbf{u}_{\varepsilon}) : \mathbb{D}(\tilde{\mathbf{u}}) - \int_{\Omega} p_{\varepsilon} \nabla \cdot \tilde{\mathbf{u}} = \int_{\Omega} \mathbf{f} \cdot \tilde{\mathbf{u}}, & \forall \tilde{\mathbf{u}} \in H_0^1(\Omega), \\ \int_{\Omega} q \nabla \cdot \mathbf{u}_{\varepsilon} = 0, & \forall q \in L_0^2(\Omega), \end{cases} \quad (\text{S7})$$

It has been proven in [27, 38] that the penalty method converges linearly in ε .

Contact algorithm

In the present hydrodynamic framework, it is known that contacts are not supposed to happen (see [21, 25]). Yet in actual simulations, collisions between particles are likely to occur because of the numerical error. The treatment of possible overlaps is crucial in the case of dense suspensions. To address this issue, we have extended to wet ellipses the numerical method already proposed for dry spheres [37]. The method consists of projecting the velocity field onto some convex admissible set depending on the current configuration, so that particles do not overlap. Since no analytical expression of the minimal distance between two ellipses is available, an approximation of this distance must be computed at each time, by solving the problem of searching for the proximal points on a each pair of ellipsoidal particles.

Let us detail the method in the case of spherical particles: we denote by $\mathbf{X}^n := (\mathbf{x}_i^n)_{i=1, \dots, N}$ the position of N particles (more precisely, the position of their gravity centre) at time t_n , and by $\hat{\mathbf{V}}^n$ their *a priori* velocity. We define the set

$$K(\mathbf{X}^n) = \{\mathbf{V} \in \mathbb{R}^{2N}, D_{ij}(\mathbf{X}^n) + \Delta t \mathbf{G}_{ij}(\mathbf{X}^n) \cdot \mathbf{V} \geq 0, \forall i < j\}, \quad (\text{S8})$$

where

$$D_{ij}(\mathbf{X}^n) = |\mathbf{x}_i^n - \mathbf{x}_j^n| - 2R_b$$

denotes the signed distance between two spheres B_i and B_j and

$$\mathbf{G}_{ij}(\mathbf{X}^n) = \nabla D_{ij}(\mathbf{X}^n) = (\dots, 0, -\mathbf{e}_{ij}^n, 0, \dots, 0, \mathbf{e}_{ij}^n, 0, \dots), \quad \mathbf{e}_{ij}^n = \frac{\mathbf{x}_j^n - \mathbf{x}_i^n}{|\mathbf{x}_j^n - \mathbf{x}_i^n|}$$

is the gradient of the distance. In order to avoid overlapping, the following splitting procedure is proposed: in a first step, we solve the variational problem without taking into account the possible overlapping of the particles (thus defining an *a priori* velocity of the spheres), then compute the projection of this *a priori* velocity onto the set of admissible velocities defined by (S8). The constrained problem is formulated as a saddle-point problem, by using the introduction of Lagrange multipliers:

$$\left\{ \begin{array}{l} \text{Find } (\mathbf{V}^n, \boldsymbol{\Lambda}^n) \in \mathbb{R}^{2N} \times \mathbb{R}_+^{N(N-1)/2} \text{ such that} \\ \mathcal{J}(\mathbf{V}^n, \lambda) \leq \mathcal{J}(\mathbf{V}^n, \boldsymbol{\Lambda}^n) \leq \mathcal{J}(\mathbf{V}, \boldsymbol{\Lambda}^n), \quad \forall (\mathbf{V}, \lambda) \in \mathbb{R}^{2N} \times \mathbb{R}_+^{N(N-1)/2}, \end{array} \right.$$

with the following functional:

$$\mathcal{J}(\mathbf{V}, \lambda) = \frac{1}{2} \left| \mathbf{V} - \hat{\mathbf{V}}^n \right|^2 - \sum_{1 \leq i < j \leq N} \lambda_{ij} (D_{ij}(\mathbf{X}^n) + \Delta t \mathbf{G}_{ij}(\mathbf{X}^n) \cdot \mathbf{V}).$$

Notice that the number of Lagrange multipliers corresponds to the number of possible contacts. In particular, if there is no contact between particles i and j , then $\Lambda_{ij} = 0$ and the Lagrange multiplier is not activated; conversely, if there is a contact between the two spheres, then Λ_{ij} may be positive and the corresponding auxiliary field allows the velocity field to satisfy the no-overlapping constraint. The approximate reaction fields $\boldsymbol{\Lambda}^n = (\Lambda_{ij}^n)$ is the dual component of a solution to the associated saddle-point problem. This problem is solved by an Uzawa algorithm (see, e.g., [12]).

In the case of ellipsoidal particles, the minimal distance between two ellipses is computed at each time by solving the problem of searching for the proximal points on a each pair of ellipsoidal particles. This problem can be defined in the following way : for all $i < j$, find $(\mathbf{x}_i, \mathbf{x}_j) \in \mathbb{R}^2$ such that

$$\begin{aligned} \mathbf{x}_i^n &\in \partial B_i, \\ \mathbf{x}_j^n &\in \partial B_j, \\ \mathbf{n}_i \cdot \mathbf{n}_j &= -|n_j| |n_i|, \\ \frac{\mathbf{n}_i}{|n_i|} &= \frac{\mathbf{x}_i^n \mathbf{x}_j^n}{|\mathbf{x}_i^n \mathbf{x}_j^n|}, \end{aligned}$$

where \mathbf{n}_i and \mathbf{n}_j are respectively the outward normal to ellipse B_i at point \mathbf{x}_i^n and the outward normal to ellipse B_j at point \mathbf{x}_j^n . We use a Newton algorithm to numerically solve this problem. The method then consists of projecting the translational but also the angular velocity onto the set of admissible velocities associated to the current configuration.

PAIR CORRELATIONS

In the main text, we have shown that active particles are able to generate rolls, related to a coherent motion. In Fig. S5 we show the pair correlation of the particles, which is the order parameter that measures the level of coherent directional motion of the velocity field [13]. The field is defined as

$$g(r) = \left\langle \frac{\mathbf{v}(\mathbf{x}, t) \cdot \mathbf{v}(\mathbf{x} + \mathbf{r}, t)}{|\mathbf{v}(\mathbf{x}, t)| |\mathbf{v}(\mathbf{x} + \mathbf{r}, t)|} \right\rangle_{p,t}, \quad (\text{S9})$$

where $\langle \rangle_{p,t}$ indicates average over time and over all particles. The pair-correlation points to the local organisation of the system, and indicates that active particles are able to manifest a certain level of coherence up to a certain integral length. The figure explains the qualitative picture discussed in the main text, as Pushers shows a higher degree of organisation up to a larger length, about $0.3L$, whereas Pullers are less correlated and only on a smaller scale, about $0.2L$. Provided hydrodynamic interactions are effective $\phi \gtrsim 0.15$, the effect of the concentration is not strong and clearly negligible for the case of pullers.

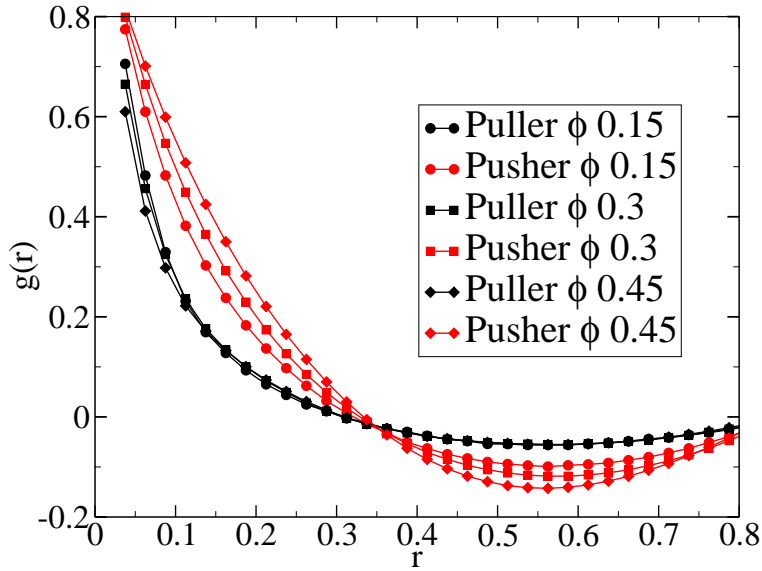


FIG. S5. Two-point particle correlation computed for active ellipsoidal particles. Pushers are in red and Pullers in black.

RHEOLOGICAL PROPERTIES

The effective viscosity of a suspension of passive spherical particles in a fluid of viscosity μ depends on its volume fraction ϕ . In the dilute regime, where $\phi \ll 1$ so that particles do not interact, the effective viscosity is well described by Einstein's relation $\mu_{\text{eff}} \approx \mu_0(1 + \alpha\phi)$, where α is known as Einstein's coefficient [3] and depends on the dimension and on the elongation of entities. The linear dependency with respect to volume fraction is due to the fact that, in this regime, the total effect of the particles on the viscosity is equal to the sum of individual contributions. Beyond the dilute regime, particles interact and thus simple addition of contributions is no more valid. Polynomial development of the form: $\mu_{\text{eff}} \approx \mu_0(1 + \alpha\phi + \beta\phi^2 + \dots)$ is needed. We have computed the effective viscosity in active suspensions of pusher- and puller-like swimmers using 2D simulations in which shear is imposed through non homogenous Dirichlet conditions and periodic boundary conditions are imposed on the left and right boundaries. We have considered concentrations up to little less than 45% volume fraction. In the main text, we have shown that three ingredients are needed in order for self-propelled swimmers to produce a rheological signature: propulsion, elongation and hydrodynamic interactions. The explanation has been already given [22, 52], and our numerical simulations naturally retrieve these mechanisms. A single active particle (pusher or puller) rotates with the same angular velocity as a passive particle of same shape, while performing an ellipsoidal trajectory with characteristics depending on its individual velocity and elongation. The contribution to apparent viscosity due to its activity depends on the orientation of the force dipole. The contribution of an active particle to apparent viscosity is maximal when the dipole of propulsion forces is against the flow, and it is minimal when this dipole helps the flow. But since the time spent by a particle in each orientation is symmetric with respect to the neutral position (when the dipole is oriented parallel to the walls and apparent viscosity is equal to the passive case), the contribution to viscosity due to the activity vanishes when averaging over one period. Thus we obtain the same effective viscosity as in the passive case. In the dilute regime, since effective viscosity is a result of the sum of contributions of each particle, self-propulsion has no impact on the rheology of the suspension. Beyond the dilute regime, hydrodynamic interactions disrupt the rotational behavior of individual swimmers. However, in the absence of a particular alignment of the active particles in the flow, the orientation of the population remains isotropic when averaging in time, and thus the effective viscosity remains the same as in the passive case. In the case of spherical active particles, there are no particular alignments and thus the activity of the particles has no impact on the effective viscosity. This is no longer true when the particles are elongated. Indeed, Fig. 3 of the main text shows the probability density function (pdf) of particle

orientations obtained for the simulations with spherical and elongated particles, in the passive and in the active case. We see that the symmetry with respect to the neutral orientation is broken in the case of active and elongated particles. Due to interactions with the other particles, the latter tend to align in the flow at an orientation that maximizes their contribution to apparent viscosity in the case of pullers, and minimizes this contribution in the case of pushers. Thus effective viscosity is enhanced in the first case, and diminished in the second case. We have also investigated how the effective viscosity evolves when the ratio between activity of the micro swimmers and shear rate changes, notably at varying the propulsion activity. For that purpose we introduce a non-dimensional number that characterizes the shear flow in presence of micro-swimmers : $\Phi = \frac{f_p}{\mu S}$, where f_p is the magnitude of the propulsion force, μ is the viscosity of the fluid and S the speed of the plates. As shown in Fig. S6, for low values of the propulsion-shear ratio, the effective viscosity in pusher (resp. puller) suspensions decreases (resp. increases) in a non-linear way. But above a certain ratio, the effective viscosity stagnates, which is consistent with what found in the literature [22, 35, 52].

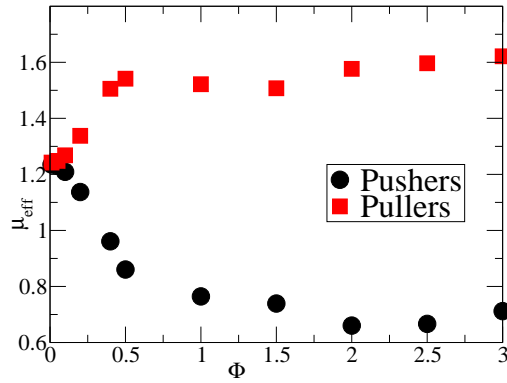


FIG. S6. Effective viscosity μ_{eff} with respect to Φ .